Astron. Astrophys. 357, 909–919 (2000)

ASTRONOMY AND ASTROPHYSICS

Rosat HRI observations of the open cluster NGC 2516

G. Micela[1], **S. Sciortino**[1], **R.D. Jeffries**[2], **M.R. Thurston**[3], **and F. Favata**[4]

[1] Osservatorio Astronomico di Palermo, Palazzo dei Normanni, 90134 Palermo, Italy (gmicela,ssciortino@oapa.astropa.unipa.it)
[2] Department of Physics, Keele University, Keele, Staffordshire, ST5 5BG, UK (rdj@astro.keele.ac.uk)
[3] School of Physics and Astronomy, University of Birmingham, Birmingham, B15 2TT, UK (mrthurston@clara.co.uk)
[4] Astrophysics Division – Space Science Department of ESA, ESTEC, Postbus 299, 2200 AG Noordwijk, The Netherlands (ffavata@astro.estec.esa.nl)

Received 28 January 2000 / Accepted 14 March 2000

Abstract. We present ROSAT HRI observations of the NGC 2516, a young southern open cluster with low metallicity. We detect 73 X-ray sources already detected with the PSPC and 12 new X-ray sources. The higher HRI spatial resolution allows us to improve the position of the previous known sources, and to better determine the optical counterparts of X-ray sources with respect to the PSPC data.

We find 28 sources with no catalogued counterparts, most with faint objects within their X-ray positional error circle. Multiband CCD photometry of these possible counterparts shows that about half of them are consistent with being dK and dM cluster members. Assuming that they are true NGC 2516 members, the derived X-ray luminosity is consistent with that observed in dK and dM stars in more metal-rich open clusters of similar age, suggesting that the activity level at which X-ray saturation occurs is insensitive to a change of a factor two in stellar metallicity.

Key words: Galaxy: open clusters and associations: individual: NGC 2516 – stars: coronae – X-rays: stars

1. Introduction

Standard stellar structure theory has been very successful in explaining the general features of stellar evolution (such as the shape of the H-R diagram, etc.). However, standard models fail to explain several observed important features in the evolution of low-mass (i.e. F, G and K-type) stars, such as the observed photospheric lithium abundance, which is a very sensitive probe of the mixing of surface and deeper layers in stars. Given the influence of metallicity (Z) on the structure of the convection zone, comparison of the evolution of well-defined stellar populations of different Z (with factors of 2 in Z making a significant difference in the convective depth) can be an effective way to determine the presence of additional mixing mechanisms and discover the time scales upon which they operate. Open clusters, consisting of stars of the same age and composition, are the ideal samples on which to perform such investigations.

Send offprint requests to: G. Micela

NGC 2516 can be a cornerstone for these studies because of its low metal abundance and closeness. Cameron (1985) reports [Fe/H] = -0.422 based on photometry. Jeffries et al. (1997) have photometrically determined the abundance of NGC 2516 to be $Z = 0.5 \times Z_{\odot}$, or $[\mathrm{Fe/H}] = -0.32$ from the presence of a $U-B$ color excess. Jeffries et al. (1998) find [Fe/H]=-0.18 ± 0.05 comparing the $B-V$ versus $V-I_{\mathrm{C}}$ plot of the cluster with the ZAMS loci derived by Pinsonneault et al. (1998) calibrated on the Hyades and Pleiades. However it is worth stressing that no direct spectroscopic abundance determination for NGC 2516 yet exists.

The photometric derived abundance, the distance (m - M=7.94) and the age ($\simeq 140$ Myr), make NGC 2516 the low metallicity counterpart of the Pleiades (age $\simeq 100$ Myr with solar metallicity). The comparison of the X-ray properties of these two clusters is a powerful method to investigate how abundances affect mixing and dynamo action in the convection zones of low mass stars.

The low Z is expected to produce well defined changes in observable properties of NGC 2516 members with respect to solar metallicity stars. The lower opacity is expected to shift the onset of convection toward lower masses, and therefore to shift the onset of magnetic activity from F3-F5 (typical for solar Z) down to F8-G0. Stars with same mass, but different metallicity have different convection zone depths, and therefore should have different dynamo efficiencies. Since loss of angular momentum is due to the magnetic braking, rotational velocity is also expected to be influenced by the lower Z. Plasmas with similar temperature structure and density, but different metallicity, have very different radiative output, since much of the broad band soft X-ray emission results from line emission (bound-bound transitions) of highly ionized elements. Hence higher metallicity stars may show enhanced X-ray emission with respect to older metal poor stars, under the same thermodynamic conditions of the coronal plasma. This effect is very strong for coronal temperatures of the order of 10^6 K (more than 95% of the emission in ROSAT band is due to bound-bound and bound-free transitions) and less relevant for hotter coronae (at 10^7 K the fraction of emission due to bound-bound and bound-free transitions is of the order of 60%), and drops very rapidly for even hotter

Table 1. Summary of the HRI observations

Field	RA(J2000) (h m s)	DEC(J2000) ° ′ ″	LIVE-TIME (sec)	UT START DATE	UT END DATE
1	7 58 07.2	−60 45 36.0	24 849	27-DEC-96/11:42:06	20-JAN-97/05:05:28
2	″	″	53 318	14-JUN-97/01:53:24	29-SEP-97/20:32:22

coronae (cf. Micela et al. 1992). Of course changes of radiative losses affect the differential emission measure of the plasma, which is governed by the balance between heating, conduction, and radiative losses.

NGC 2516 has been observed with the ROSAT Position Sensitive Proportional Counter (PSPC) with two observations of ~ 10 ksec (Dachs & Hummel 1996) and 60 ksec (Jeffries et al. 1997, Paper I), respectively. These fields are very crowded, and in the longest exposure more than 160 X-ray sources have been detected (Paper I), with the majority of the sources concentrated in the central part of field of view, as shown in Fig. 4 of Paper I. Many of the sources are confused and the fluxes have been evaluated by fitting multiple PSF's to the data. This method allowed reliable fluxes to be obtained for the most intense sources, but was less reliable for the weaker sources, some of which are likely missed since they would be too close to very bright sources. Another problem for such a field that is rich in both X-ray sources and their possible optical counterparts, is that frequently more than one optical candidate falls within the error circle of a PSPC X-ray source. We note that in the deepest exposure, the PSPC reached fluxes as faint as $10^{-14}\mathrm{erg\ sec^{-1}cm^{-2}}$. Considering that in young clusters, the most active late-type stars have a $\log(f_X/f_V)$ ratio in the range -2 to -1, the corresponding optical counterparts could have V between 16.3 and 18.7. Hence a good spatial resolution is required in order to properly and unambiguously identify the true counterparts of X-ray sources and to correctly determine the X-ray properties of the cluster, especially among the lower mass stars.

The PSPC observations of NGC 2516 in Paper I gave a number of indications about the effects of abundance on X-ray emission: the authors found that a group of F stars have an emission level higher than the maximum emission observed in the stars *of same color* in the Pleiades: a possible explanation of this effect is that metal poor stars in the considered color range have lower mass than metal rich stars and hence thicker convection zones. Indeed the effect vanishes if stars of same mass range (and not color!) are compared (cf. Fig. 12 of Paper I). The G stars in NGC 2516 are in fact X-ray underluminous with respect to their counterparts in the *older* NGC 6475 cluster, suggesting a dependence of the activity-rotation paradigm on metallicity. On the other hand lithium depletion should also depend on the properties of the convection zone, but lithium in NGC 2516 does not behave as expected on the basis of standard models (Jeffries et al. 1998), casting doubt both upon the real effects of metallicity on the convection zone, and upon mixing mechanisms in general. Alternatively it is possible that the metallicity of NGC 2516, obtained from photometric observations, is underestimated and that the metallicity of the cluster is close to solar.

In this paper we present the results of a ~ 80 ksec observation obtained with the High Resolution Imager (HRI – Zombeck et al. 1990) onboard ROSAT. Two separate observation sequences were obtained in the same direction as the PSPC observations described in Paper I. The sky region covered by the HRI is ~ 38 arcmin diameter, covering only the central portion of the PSPC observation. The efficiency of the detector is lower than that of the PSPC, hence the present observations should be less sensitive than the PSPC one, but the higher spatial resolution should allow us to better identify the sources and to limit confusion problems, and to compensate, at least in the center of the field of view, for the loss of sensitivity (since the narrow HRI PSF makes it possible to have a smaller detection cell with fewer background counts).

We note that because of its rich X-ray source population, NGC 2516 has been selected as calibration target for the Chandra and XMM instrumentation. It is therefore important to accurately obtain X-ray source positions as well as the positions of their counterparts in order to calibrate the spatial resolution capability of Chandra and XMM.

Our paper is organized as follows: Sect. 2 presents the observations and data analysis, Sect. 3 presents the identifications of the X-ray detections, Sect. 4 discusses the properties of sources unidentified with catalogued objects together with photometric observations of their possible counterparts, and Sect. 5 compares fluxes obtained with the present observations with those obtained with PSPC in order to assess coronal variability in NGC 2516 on timescales of years.

2. X-ray observations and data analysis

The observations have been performed in two pieces separated by about six months; in Table 1 we report the journal of the observations. We have analyzed the two HRI images individually and then we have summed them up in order to achieve the highest sensitivity. Both segments have been obtained over a large elapsed time (about one month for the first and more than three months for the second), limiting the possibility of exploring variability on time scales of hours or few days. The observational timing is well suited to explore variability on time scales of weeks and few months, but the low statistics of the sources prevents it.

As a detection algorithm we have adopted the wavelet transform algorithm developed by Damiani et al. (1997a), tuned for the HRI (see Micela et al. 1999 for details). We have constructed a flat field using the exposure map, which takes into account

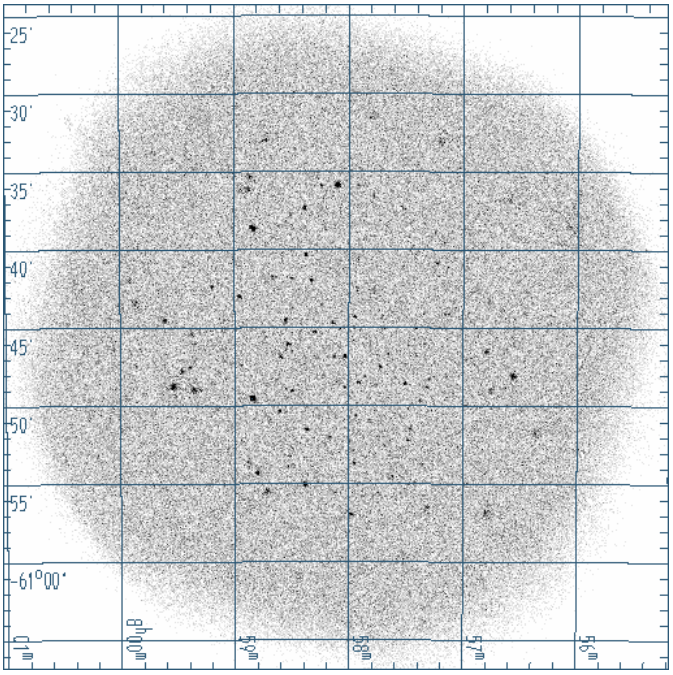

Fig. 1. Summed HRI image of central region of NGC 2516.

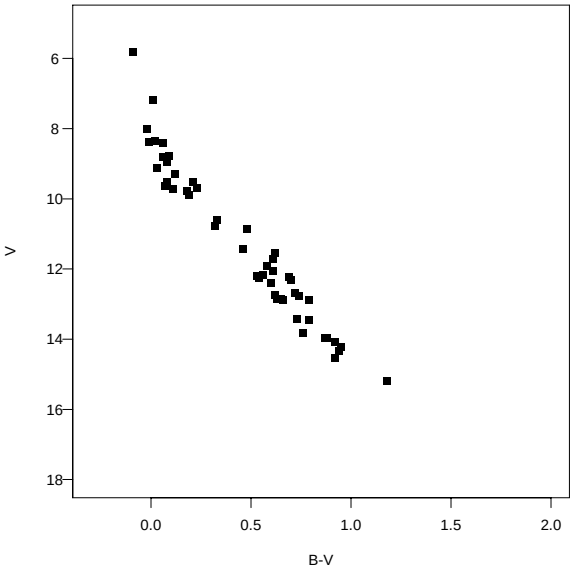

Fig. 2. HR diagram of catalogued cluster members detected in the HRI observation.

the vignetted cosmic X-ray background and the intrinsic detector nonuniformities. We also constructed a particle background map, that accounts for the increase of the particle-induced background at large off-axis angles and which contributes a substantial fraction of the total observed background (Snowden et al. 1994, Snowden 1998).

The detection threshold has been chosen so that we detect only $\sim$1 spurious source per field. For our exposure times this threshold corresponds approximately to a gaussian equivalent (i.e. same probability as the normal distribution with this value) of 4.5 σ. Since the number of photons per HRI resolution element is small, and hence the statistics are far from the gaussian limit, a large number of simulations were performed to determine the proper acceptance threshold.

As a first step we applied the detection algorithm to the two images separately. This enables us to identify possible systematic offsets due to limitations in the ROSAT aspect determination, which can be of the same order as the spatial resolution of the HRI. After a first identification process with catalogued stars (see below) we found that both segments had small systematic offsets ($\sim 2''$ in the first segment and $\sim 4''$ in the second one). In order to sum up the two segments we properly registered the two individual observations, and then ran the detection algorithm on the summed image, finding a total of 83 X-ray sources. The summed image is shown in Fig. 1, while the final source list is reported in Table 2. At the end of the table we have added two sources that were detected in the second segment, but were not detected in the summed image for intrinsic variability or for statistical fluctuations. Source # 77 is likely spurious as discussed below.

For each source we report the coordinates, the detection significance in equivalent σ (i.e., same probability as the normal distribution with this value), the count rate (and error) computed from the counts obtained by the detection algorithm and the observation times measured from the exposure map, the 50% and 90% error circles according to the analytical formulation of Damiani et al. (1997a, see also Sciortino et al. 1998), the PSPC counterpart (JTX sources from Paper I) of HRI sources, and an optical identification flag. In order to cross-correlate HRI and PSPC sources we have assumed the 90% error circle for the former and $15''$ for the latter (see Paper I). In 95% of the matches we obtain, the offset between HRI and PSPC sources is smaller than $15''$.

We note that we have detected 12 new X-ray sources that were not detected with the PSPC in Paper I.

3. Identifications

We have identified our detected sources with the PSPC sources (JTX list in Paper I), with the cluster members from the optical catalog compiled in Paper I, mainly on the basis of Dachs & Kabus (1989) and Eggen (1972) and with Simbad catalogued objects. As a first step we adopted an identification radius equal to the 50% positional uncertainty computed by the detection algorithm. If no counterpart is present in the above error circle, we have adopted the 90% error circle. In the identification process with JTX sources we have added an uncertainty of $15''$ in quadrature to allow for the uncertainty in the positions of the PSPC sources. Using this criterion we have identified 73 of the JTX sources. Out of the 85 HRI sources 47 are identified with catalogued cluster members, 10 with field stars and 28 sources are unidentified with catalogued objects. The identifications with the cluster members are in general very good, with $\sim$90% of the identifications within $6''$. We report in Table 3 the X-ray properties of cluster members we have detected, while Fig. 2 shows the HR diagram for these sources. Detected members, as already found in Paper I, cover the whole mass

Table 2. X-ray sources detected in the ROSAT-HRI observation. For each source we report the coordinates, the off-axis angle, the detection significance (in equivalent σ i.e. same probability as the normal distribution with this value), the count rate with its error, the 50% and 90% positional uncertainty, and the identification with PSPC sources in Paper I, the source D32 is not detected in Paper I, but it is detected in Dachs & Hummel 1996. A flag in the last column indicates if the source is identified with a cluster member (C), with a field star (F) or is not identified with catalogued object (N)

#	R.A.(J2000) (h. m. s.)	DEC.(J2000) ° ′ ″	Off-axis ′	σ	Rate cnt/ksec	Err	Pos.Err . 50%[″]	90%[″]	JTX	ID
1	7:56:03.0	−60:38:21.8	17.0	4.75	2.16	0.64	20.0	35.4	4	N
2	7:56:22.0	−60:51:47.8	13.7	7.75	1.59	0.39	13.9	25.7	12	C
3	7:56:33.9	−60:48:08.3	10.5	14.57	2.19	0.25	9.4	18.8	16	F
4	7:56:34.4	−60:36:48.3	13.4	5.77	2.32	0.61	14.3	24.4	...	N
5	7:56:45.8	−60:49:03.8	8.9	6.67	0.70	0.19	7.7	16.5	22	C
6	7:56:46.3	−60:43:23.8	8.4	4.85	0.68	0.21	7.3	15.9	23	N
7	7:56:47.8	−60:56:53.9	13.7	8.72	2.26	0.39	15.2	27.7	25	C
8	7:56:47.9	−60:46:33.9	7.9	9.77	1.05	0.18	6.8	15.3	26	N
9	7:57:11.9	−60:33:09.7	14.0	6.14	0.91	0.26	14.0	25.7	35	F
10	7:57:13.7	−60:40:54.7	7.7	7.99	0.50	0.15	5.0	13.1	36	C
11	7:57:18.3	−60:48:19.8	6.0	5.45	0.39	0.12	3.8	11.9	...	N
12	7:57:19.1	−60:56:32.3	12.1	6.47	0.68	0.19	10.5	20.4	38	N
13	7:57:19.3	−60:48:49.8	6.1	5.64	0.41	0.13	3.9	12.0	39	C
14	7:57:23.0	−60:49:42.4	6.1	6.29	0.47	0.14	4.0	12.0	41	F
15	7:57:25.2	−60:45:02.4	4.2	6.81	0.52	0.16	3.1	11.3	43	N
16	7:57:28.4	−60:51:30.0	6.9	5.84	0.79	0.22	4.5	12.6	...	C
17	7:57:29.1	−60:52:15.0	7.5	6.37	0.36	0.12	5.0	13.1	46	N
18	7:57:30.9	−60:48:35.1	4.4	10.99	0.87	0.14	3.1	11.3	50	C
19	7:57:31.8	−60:37:22.6	8.8	4.76	0.47	0.15	6.3	14.7	52	C
20	7:57:38.0	−60:54:35.2	9.2	5.49	0.75	0.22	6.6	15.0	54	C
21	7:57:43.9	−60:47:30.2	2.0	9.11	0.66	0.12	2.4	10.8	62	C
22	7:57:47.0	−60:42:40.3	3.0	4.51	1.16	0.36	2.6	10.9	64	N
23	7:57:47.1	−60:36:35.3	9.0	5.05	0.50	0.16	6.4	14.7	66	C
24	7:57:47.8	−60:31:25.3	14.2	5.72	1.17	0.32	14.4	26.4	67	C
25	7:57:49.3	−60:51:00.3	5.4	4.93	0.48	0.15	3.3	11.5	...	N
26	7:57:51.7	−60:48:07.8	2.6	4.94	0.26	0.09	2.4	10.8	...	N
27	7:57:55.2	−60:48:30.3	3.1	8.94	0.69	0.13	2.4	10.8	72	C
28	7:57:55.2	−60:35:52.8	9.8	4.52	0.33	0.12	7.0	15.5	71	N
29	7:57:55.9	−60:42:40.3	3.1	4.51	0.24	0.10	2.4	10.8	74	N
30	7:57:55.9	−60:42:32.8	3.2	4.87	0.47	0.15	2.5	10.9	74	N
31	7:57:56.5	−60:50:37.9	5.2	5.52	0.30	0.10	3.0	11.2	75	C
32	7:57:57.2	−60:44:17.8	1.8	10.20	0.73	0.12	2.2	10.7	78	C
33	7:57:57.5	−60:53:42.9	8.2	6.82	0.52	0.14	5.1	13.2	77	C
34	7:57:59.2	−60:56:57.8	11.5	9.98	0.98	0.17	8.9	18.1	80	C
35	7:58:00.3	−60:52:15.3	6.7	5.72	0.57	0.17	3.9	12.0	81	N
36	7:58:02.4	−60:46:50.4	1.3	13.92	1.21	0.16	2.2	10.7	84	C
37	7:58:02.7	−60:48:50.4	3.3	5.74	0.31	0.10	2.4	10.8	82	C
38	7:58:05.1	−60:45:05.4	0.5	4.79	0.25	0.09	2.1	10.6	85	C
39	7:58:06.1	−60:35:52.9	9.7	28.88	3.90	0.26	6.8	15.3	86	N
40	7:58:08.2	−60:46:52.9	1.4	6.73	0.51	0.14	2.1	10.6	...	C
41	7:58:08.8	−60:44:42.9	1.1	7.36	0.56	0.16	2.1	10.6	88	C
42	7:58:10.2	−60:52:00.4	6.5	7.32	0.43	0.13	3.7	11.8	89	C
43	7:58:14.6	−60:35:55.4	9.8	6.87	0.53	0.15	6.8	15.2	D32	N
44	7:58:14.6	−60:43:32.8	2.6	4.56	0.32	0.11	2.2	10.7	94	C
45	7:58:16.3	−60:30:15.3	15.5	4.68	0.52	0.17	16.6	29.8	...	N
46	7:58:18.0	−60:45:17.9	2.2	9.12	0.77	0.14	2.2	10.7	95	C
47	7:58:19.7	−60:41:57.8	4.4	9.24	0.85	0.14	2.6	10.9	96	C
48	7:58:22.2	−60:51:32.8	6.6	16.29	1.47	0.16	3.6	11.7	97	C
49	7:58:22.8	−60:40:20.3	6.0	13.56	1.15	0.15	3.3	11.5	99	F
50	7:58:23.2	−60:55:02.8	9.9	15.08	1.77	0.21	6.5	15.0	100	C
51	7:58:23.4	−60:37:20.3	8.8	11.47	1.15	0.17	5.5	13.6	101	F
52	7:58:26.7	−61:00:55.3	15.7	4.52	0.69	0.22	16.5	29.7	...	N

Table 2. (continued)

#	R.A.(J2000) (h. m. s.)	DEC.(J2000) ° ′ ″	Off-axis ′	σ	Rate cnt/ksec	Err	Pos.Err . 50%[″]	90%[″]	JTX	ID
53	7:58:30.0	−60:49:05.2	5.4	8.45	0.68	0.18	2.7	11.0	102	N
54	7:58:30.3	−60:41:50.2	5.7	6.32	0.35	0.11	2.9	11.1	103	C
55	7:58:30.9	−60:37:45.2	9.0	5.18	0.50	0.15	5.3	13.5	104	C
56	7:58:31.4	−60:53:15.2	8.8	4.59	0.33	0.11	5.1	13.2	105	C
57	7:58:32.0	−60:46:05.2	4.5	10.27	0.84	0.21	2.4	10.8	107	F
58	7:58:33.4	−60:44:30.2	4.9	10.08	0.78	0.14	2.4	10.8	108	C
59	7:58:35.8	−60:46:55.2	5.3	11.36	0.89	0.13	2.5	10.9	109	C
60	7:58:36.6	−60:50:22.7	7.1	8.95	0.72	0.14	3.4	11.6	111	C
61	7:58:40.2	−60:41:47.6	7.0	6.24	0.61	0.18	3.2	11.4	113	C
62	7:58:43.1	−60:55:30.1	11.8	9.51	1.35	0.23	8.0	17.0	114	C
63	7:58:44.1	−60:33:00.0	14.2	6.61	0.72	0.20	12.4	23.3	116	C
64	7:58:48.3	−60:54:20.0	11.4	11.03	1.17	0.21	7.0	15.5	119	C
65	7:58:50.6	−60:38:37.4	10.4	23.74	3.38	0.27	5.7	13.9	122	C
66	7:58:50.9	−60:49:32.4	8.7	50.20	8.58	0.36	3.8	11.9	121	C
67	7:58:52.3	−60:35:19.9	13.0	7.88	1.13	0.29	9.4	18.9	123	N
68	7:58:52.7	−60:53:39.9	11.4	5.67	0.79	0.23	6.7	15.2	124	C
69	7:58:53.0	−60:36:09.9	12.4	7.81	0.82	0.22	8.4	17.4	126	C
70	7:58:56.6	−60:47:24.8	8.9	4.67	0.25	0.09	3.6	11.7	...	N
71	7:58:57.6	−60:43:02.3	9.2	9.49	0.87	0.15	3.9	12.0	131	F
72	7:59:12.2	−60:42:24.4	9.2	8.44	0.66	0.17	5.5	13.6	137	N
73	7:59:18.6	−60:31:39.2	17.0	5.15	2.29	0.65	19.1	33.9	...	N
74	7:59:21.3	−60:48:59.1	10.8	10.53	1.57	0.25	6.6	15.0	139	C
75	7:59:22.9	−60:45:26.5	10.5	6.74	0.69	0.19	6.1	14.5	140	C
76	7:59:23.6	−60:47:34.0	10.8	7.17	0.56	0.16	6.5	14.8	141	F
77	7:59:25.3	−60:47:33.9	11.1	4.92	1.29	0.39	6.7	15.1	143	N
78	7:59:27.7	−60:47:48.9	11.5	8.11	0.87	0.22	7.1	15.7	143	C
79	7:59:32.2	−60:48:48.7	12.5	17.13	2.46	0.26	8.1	17.0	144	C
80	7:59:36.8	−60:44:33.5	12.9	10.19	1.02	0.17	8.3	17.4	147	F
81	7:59:52.0	−60:47:27.8	15.5	4.57	0.35	0.12	11.4	21.8	...	N
82	7:59:52.4	−60:43:27.8	15.6	7.37	1.10	0.28	11.6	22.1	149	N
83	7:59:55.1	−60:41:57.7	16.3	5.41	0.79	0.23	12.8	24.0	150	C
84*	7:56:59.2	−60:49:52.4	7.3	4.63	0.31	0.12	6.3	14.7	30	N
85*	8:00:04.9	−60:46:15.3	14.9	4.98	1.19	0.36	14.2	25.0	154	F

* Sources detected only in the second segment

range present in the optical catalog. X-ray luminosities have been computed assuming a conversion factor from counts to flux of $4.5\ 10^{-11}\mathrm{erg\ cm^{-2}}$/count (computed with *pimms* for a Raymond-Smith spectrum with T=0.3kev and a absorbing hydrogen column N_H=7 $\times$ $10^{20}\mathrm{cm^{-2}}$ and an intrinsic distance modulus of 7.94 for consistency with Paper I (see Sect. 5). When we found two possible counterparts, in absence of further information, we split the observed rate between them.

We find 12 sources that were not detected in Paper I. Nine cannot be identified with cataloged sources and one (#43) was detected by Dachs & Hummel (1996). The two remaining new sources are identified with cluster members, one late-type and one early-type star, respectively. The emission detected from the latter could be due to UV leak contamination through the HRI filters (Zombeck et al. 1997), but we cannot exclude real X-ray emission from this star since a significant fraction of early type stars have been detected as X-ray sources in NGC 2516 (Paper I) and the PSPC does not suffer similar UV contamination.

4. Sources without cataloged counterparts

We have detected 28 sources without catalogued counterparts. Many of these sources (18 out of 28) have been detected in at least one of the previous PSPC observations, and one of the remaining has been detected in our reanalysis of PSPC data (Micela et al. in preparation), based on a wavelet base algorithm (Damiani et al. 1997b). An inspection of the STScI Digitised Sky Survey (DSS) reveals that most of these sources have faint counterparts. In Fig. 3 we present finding charts for these 28 sources. Each finding chart is a square of 2′ of size. The circles inside the finding charts represent the 50% of positional uncertainty or, when two circles are shown, the outer one is the 90% positional uncertainty.

4.1. Expected field sources

We have computed the expected number of field sources in our fields, using the sensitivity maps obtained by the wavelet algo-

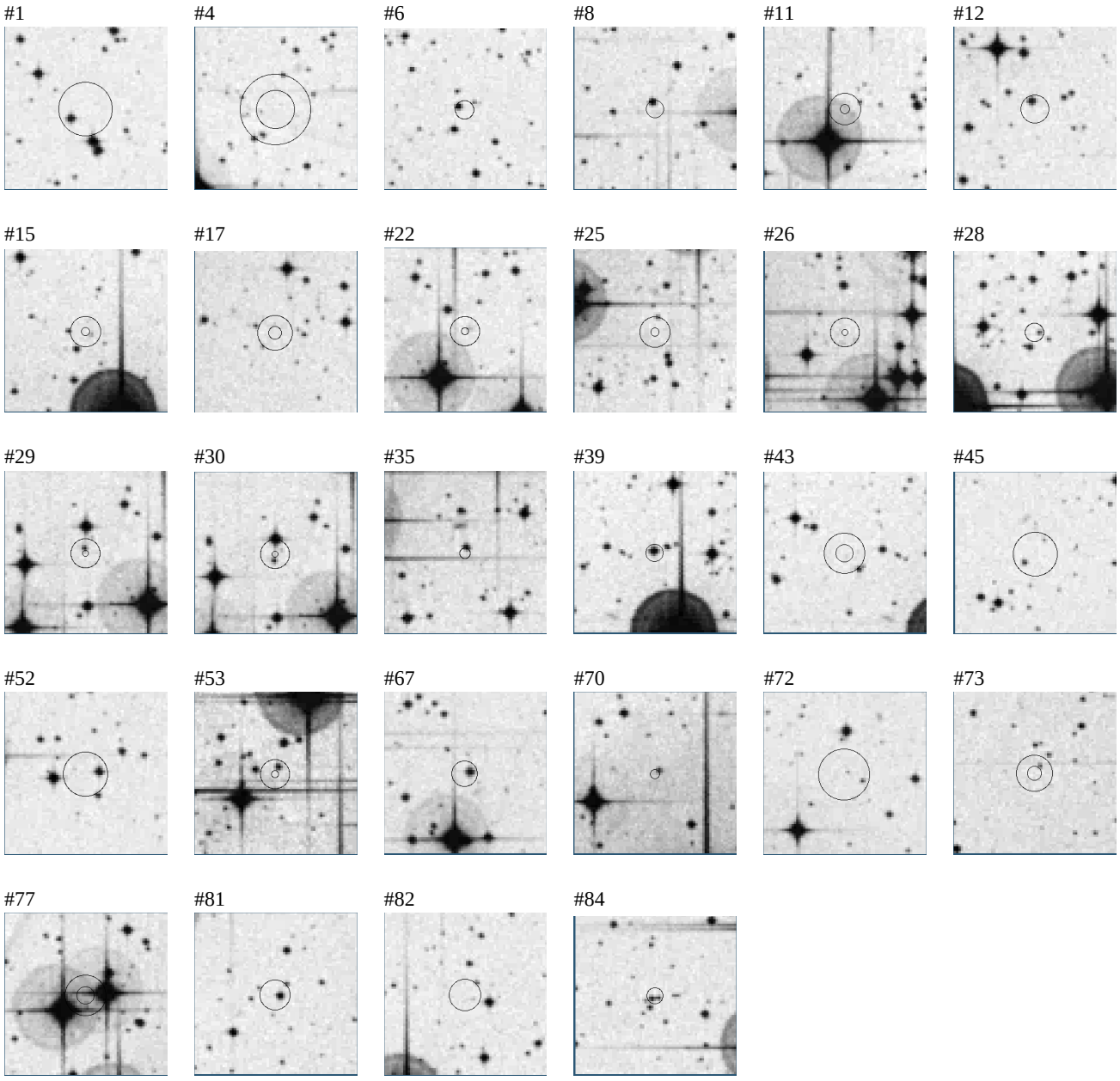

Fig. 3. Finding charts for unidentified HRI sources detected in the NGC 2516 region extracted from the STScI DSS. Each chart is $2'$ on a side, centered on the HRI position. Identification circles at 50% are indicated, if there are no counterparts in this identification circle, the 90% circle is also shown.

rithm with a spatial resolution of $10''\times10''$. Given the relatively low galactic latitude of the cluster (b$\sim -16°$) we expect a contribution both from galactic and extragalactic sources. Hence we have decided to estimate the number of field objects with two different approaches. First we have estimated the number of expected extragalactic sources from the $\log(N)$–$\log(S)$, derived at higher latitudes, of Branduardi-Raymont et al. (1994), and of Hasinger et al. (1993). We have assumed a hydrogen column $N_H = 1.2\ 10^{21}$ cm^{-2} towards NGC 2516, obtained by interpolating data from Stark et al. (1992), and a power-law spectrum with a photon index ranging between 1 and 2. The total number of sources predicted for our survey ranges between 8 and 12. Schmidt et al. (1998) find that the fraction of coronal stellar sources in the X-ray source sample in the Lockman hole (Hasinger et al. 1993) is only 6% of the total, which in our case implies that less than 1 of these predicted sources is of stellar nature.

Given the lower latitude of NGC 2516 we expect a larger number of normal stellar sources unrelated to the cluster. In order to predict them we have used the XCOUNT model (Favata et al. 1992) that allows the prediction of numbers of field stellar X-ray sources, taking into account the age dependence of coronal emission in stars and their galactic distribution. We have also used the sensitivity map obtained by the wavelet algorithm

Table 3. X-ray properties of detected cluster members. The parenthesis in L_x values indicate sources with more than one counterpart; in these cases we have assumed that all the counterparts contribute at the same level to the observed luminosity.

OPT ID	V	B-V	X-ray #	Offset [″]	log L_x [erg s^{-1}]
DK 423	11.56	0.62	2	7.5	30.11
DK 73	8.36	0.02	5	8.0	(28.46)
DK 74	8.78	0.09	5	5.8	(28.46)
DK 426	10.86	0.48	7	4.0	30.27
DK 233	12.32	0.70	10	5.0	29.61
DK 15	9.29	0.12	13	7.2	29.52
DK 463	13.46	0.79	16	1.3	29.81
E 111	14.08	0.92	18	3.1	29.85
DK 230	12.84	0.65	19	3.1	29.58
DK 23	8.81	0.06	20	5.2	29.79
DK 306	13.83	0.76	21	3.2	29.73
DK 26	8.39	−0.01	23	5.4	29.61
DK 238	12.18	0.56	24	7.3	29.98
DK 403	12.88	0.79	27	3.3	29.75
DK 503	12.67	0.72	31	4.8	29.39
DK 32	9.88	0.19	32	2.1	29.78
E 27	14.55	0.92	33	4.1	29.63
DK 513	12.84	0.63	34	4.1	29.90
DK 78	12.05	0.61	36	2.3	29.99
DK 34	8.95	0.08	37	3.6	29.40
DK 206	12.74	0.62	38	2.7	29.31
DK 82	8.4	0.06	40	2.9	29.62
DK 205	12.25	0.54	41	2.3	29.66
DK 37	9.51	0.21	42	4.6	29.55
DK 41	9.69	0.23	44	0.6	29.42
DK 902	11.44	0.46	46	0.9	29.80
DK 907	12.39	0.60	47	2.3	29.84
DK 44A	7.18	0.01	48	9.0	(29.78)
DK 44B	8.02	−0.02	48	6.9	(29.78)
DK 668	14.21	0.95	50	6.0	30.16
DK 48	9.72	0.11	54	4.5	29.46
DK 922	10.62	0.33	55	1.8	29.61
E 13	15.18	1.18	56	5.4	29.43
DK 904	12.87	0.66	58	2.4	29.80
DK 803	13.43	0.73	59	2.3	29.86
DK 86	11.7	0.61	60	3.7	29.77
DK 911	12.21	0.53	61	4.6	29.70
DK 664	13.97	0.87	62	3.6	30.04
DK 933	12.77	0.74	63	3.6	29.77
E 10	14.34	0.94	64	6.0	29.98
DK 55A	9.51	0.08	65	3.6	30.44
DK 56	5.8	−0.09	66	6.1	30.85
DK 609	12.22	0.69	68	2.4	29.81
DK 57	9.77	0.18	69	1.1	29.83
DK 62	9.11	0.03	74	2.3	30.11
DK 811	11.91	0.58	75	5.1	29.75
DK 95	9.65	0.07	78	2.6	29.85
DK 96	13.98	0.88	79	3.7	30.30
DK 66	10.77	0.32	83	4.9	29.81

in this case. We obtain a total of ~ 4 expected "normal" coronal sources plus a maximum of two RS CVn systems if we assume the high spatial density of active binaries of 4×10^{-4} pc^{-3} (Favata et al. 1995). Comparing these numbers with the number (10) of field stars detected and also considering the number of sources without cataloged counterparts, we are probably seeing an excess of detected field stars over the XCOUNT predictions, that is similar to that found in the analysis of the stellar content of the *Extended Medium Sensitivity Survey* (Sciortino et al. 1995). Furthermore, we note that NGC 2516 is just on the edge of the Gould Belt (Guillout et al. 1998) that has been shown to have an excess of X-ray bright late-type stars which is not presently modeled by XCOUNT. In particular NGC 2516 is at 12.5° from the nominal Gould Belt determined by Guillout et al. that has a thickness of 20°. It is possible that the excess X-ray sources we have found are foreground X-ray sources related to the Gould Belt population.

4.2. New identifications

We have identified the sources without published counterparts with stars from a new photometric catalog obtained by Jeffries, Thurston & Hambly (in preparation). Briefly, this catalogue results from a BVI_c CCD survey of approximately 1 square degree of NGC 2516 centered on the ROSAT pointing. These data were taken at the CTIO 0.9-m telescope during January 1995 in photometric conditions and were flat-fielded with twilight exposures. Nightly corrections for extinction and transformations to the Johnson V, $B-V$ and Cousins $V-I_C$ systems were achieved using many observations of standard fields from the Landolt (1992) compilation, including several very red stars.

Aperture photometry was performed using small apertures (3-6 arcsec radius) on a series of 25 mosaiced CCD fields, each covering an area of 13.5×13.5 arcminutes^2 at a plate scale of 0.4 arcsec/CCD pixel. Astrometry of the frames was done with reference to Guide Star Catalogue objects in the same fields. The internal accuracies of the positions are typically 0.5 arcsec. Comparison of stars in the overlapping regions of CCD fields gives us a good idea of the internal photometry errors. These range from about 0.015 mag for the brightest stars that are unsaturated in the survey ($V \simeq 11$–12) to about 0.06 mag for stars at $V = 18$–19. The catalogue of $\sim$ 15 500 stars is essentially complete (except near bright stars and CCD cosmetic defects) in V and $V-I$ to $V = 20$ and complete in V and $B-V$ to about $V = 19$. External errors are likely to be quite small. Residuals to the linear transformation functions used to fit the Landolt standards were less than 0.02 mag on all nights.

For the identifications we have used a procedure similar to that described in Sect. 3. When available we have used counterpart(s) inside the 50% error circle, otherwise those inside the 90% error circle (see Sect. 2). Adopting this criterion we identify 15 sources with a single counterpart, 7 with two counterparts, and 1 with three possible counterparts. 5 sources (# 17, 22, 26, 43, and 77) remain without counterparts down to the limiting sensitivity of the photometric observations. Source # 77 is likely a spurious source due to the presence of two close sources (# 76 and # 78).

Table 4. Photometry of the new candidate counterparts of X-ray sources. For the stars with photometry consistent with the cluster we report the L_x and L_x/L_{bol}, computed assuming that they are cluster members. The parenthesis in L_x values indicate sources with more than one counterpart among the possible members; in these cases we have assumed that the counterparts contribute at the same level to the observed luminosity.

X-ray #	V	B-V	V-I	Offset [″]	f_x/f_V	log L_x [erg s^{-1}]	log(L_x/L_{bol})
1	14.74	1.04	1.29	15.2	-1.62	30.25	-2.87
6	16.32	1.33	1.66	6.2	-1.49	(29.44)	-3.28
	18.84	1.65	2.13	6.9	-0.48	(29.44)	-2.46
8	15.41	1.27	1.55	3.5	-1.66	29.93	-3.06
12	15.12	1.18	1.48	5.1	-1.97	29.74	-3.30
25	17.80	1.47	2.13	9.3	-1.05	29.59	-2.73
28	17.64	1.71	2.84	4.5	-1.27	29.43	-3.29
29	17.17	1.52	1.91	3.0	-1.60	29.29	-3.19
35	15.76	1.41	1.71	3.0	-1.79	29.67	-3.29
53	16.18	1.43	1.83	4.2	-1.54	29.74	-3.10
67	14.78	0.99	1.13	2.6	-1.88	29.96	-3.13
70	17.18	1.49	1.93	1.6	-1.58	29.31	-3.17
84	16.56	1.35	1.91	5.8	-1.73	29.40	-3.32
4	19.96	...	0.80	23.1	+0.50		
	18.18	0.81	0.79	23.4	-0.21		
	17.98	0.78	0.98	23.7	-0.29		
11	18.57	0.97	1.06	10.2	-0.83		
15	19.72	...	1.43	5.4	-0.24		
30	17.17	1.52	1.91	7.1	-1.31		
	13.04	1.07	1.11	10.1	-2.96		
39	14.41	1.40	1.84	1.7	-1.49		
45	19.67	...	1.41	8.9	-0.26		
	17.27	0.97	1.03	13.6	-1.22		
52	20.55	...	1.94	9.3	+0.21		
	14.96	0.64	0.81	9.5	-2.02		
72	19.89	0.81	0.94	2.9	-0.07		
73	19.64	...	1.98	1.8	+0.37		
	18.15	0.92	1.12	14.0	-0.23		
81	15.77	0.80	0.81	3.6	-2.00		
	18.25	0.86	0.78	9.4	-1.00		
82	19.23	0.56	1.22	9.7	-0.11		
84	17.89	1.05	1.23	4.0	-1.20		

Table 4 reports the photometry of the counterparts of these 23 sources, while Fig. 4 reports the HR diagram for stars with B-V values, with that of cluster members detected in Paper I. The figure and table indicate that 13 of the candidate counterparts of 12 X-ray sources have photometry consistent with the low mass population of the cluster and f_x/f_V values typical of young stars. The remaining X-ray sources are surely unrelated to the cluster and their number is not much higher than the number of expected field sources.

We note that the pure chance positional matches between X-ray positions and the new photometric catalog should produce ~ 8 spurious matches down to V=19, but these would not be expected to lie near the cluster main sequence in general. The bulk of the objects identified with objects with photometry inconsistent with cluster membership have f_x/f_V values much higher than normal stars and more typical of extragalactic sources. Furthermore, if their identifications were spurious, the true counterparts will be even fainter and thus the even higher f_x/f_V values would reinforce their extragalactic nature.

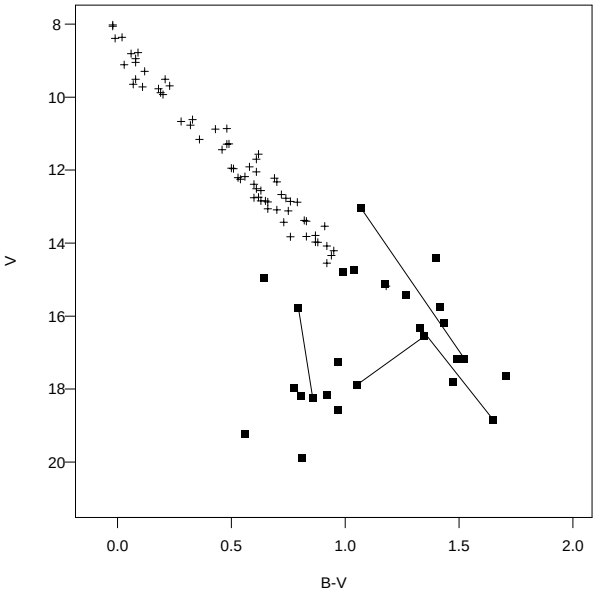

Fig. 4. HR diagram of the counterparts of "unidentified" HRI sources (filled symbols), lines connect counterparts of the same sources. Crosses indicate the cluster members detected in Paper I.

The new candidate cluster members have visual magnitudes in the range between 15 and 19 and have colours corresponding to K and M stars, where the previously catalogued NGC 2516 members were severely incomplete or non-existent. For these stars we have computed the L_x and L_x/L_{bol} values assuming the same conversion factor used in Sect. 3 for cluster members. We note that the X-ray luminosity of these stars is typically very high, on the upper tail of the X-ray luminosity functions of stars of similar spectral type in the Pleiades (Stauffer et al. 1994, Micela et al. 1996), and the L_x/L_{bol} values are typical of saturated stars.

Our results can be easily reconciled with the results of Hawley et al. (1999), although it bring us to slightly different conclusions. 10 out of the 17 JTX sources falling in the region explored by Hawley et al. (1999) are "unidentified" in Paper I and Hawley et al. are able to identify at most 4 of these 10 sources with late-type possible cluster members. Indeed a computational error in calculating the offset between X-ray and optical positions (Hawley, private communication) produced an overestimate of their offset. Using the correct computation we identify 5 of the remaining 6 sources (JTX 91 is identified with Hawley 77 with offset=19.4″; JTX 92 with Hawley F with offset=21.2″; JTX 98 with Hawley 69 with offset 15.9″; JTX 117 with Hawley 106 with offset 15.8″; JTX 118 with Hawley 28 with offset 17.8″). Two of the new identifications (Hawley 69 and Hawley 106) are possible dM cluster members, bringing up to 6 the late-type possible members. The fraction (6/10) of sources identified with possible dM cluster members by Hawley is similar to the fraction resulting in our study (12/28). The only source in the

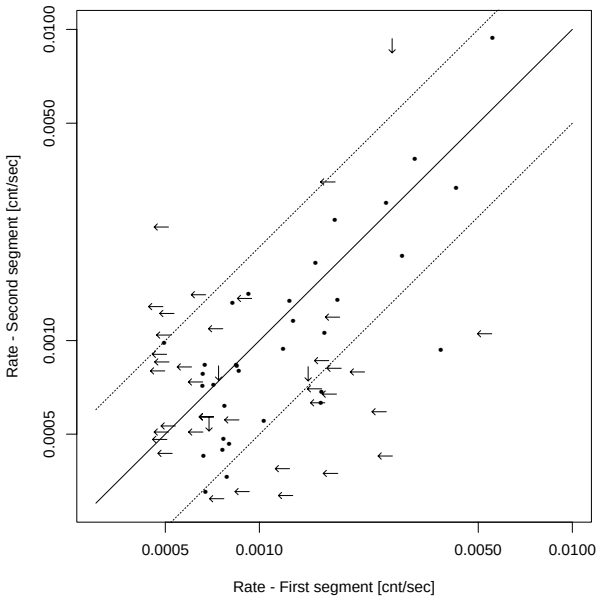

Fig. 5. Rate measured in the second segment vs. rate measured in the first one for the sources of Table 2. The continuous line indicates the identity, while dashed lines indicate variations of a factor two.

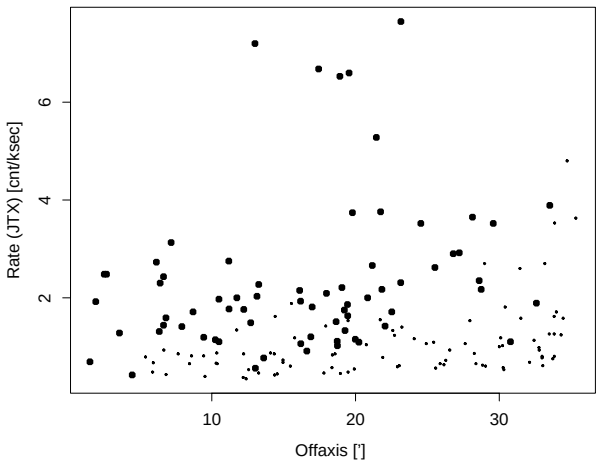

Fig. 6. PSPC rate vs. HRI offaxis angle of the PSPC source falling in HRI field of view. Large symbols indicate sources detected both in the PSPC and the HRI observation, while small symbols indicate sources detected only in the PSPC exposure and undetected in HRI field.

Hawley et al. study that remains unidentified is a small fraction of the total of X-ray sources (1/17) that compares well with our unidentified source fraction (5/85).

5. X-ray variability on medium and long time scale

5.1. Comparison between the HRI observations

Taking advantage of the time separation between the two HRI exposures we have searched for variability on a six month time scale. To this purpose we have compared the rates (both detections and upper limits) measured in the individual segments of the sources detected in the summed exposure (Table 2). In Fig. 5 we report the scatter plot of count rates measured in the two exposures.

We found 10 sources that show variations greater than a factor two. Two sources (#54 and #69) are two early type cluster members, one (#2) is a G cluster member, 4 sources (#9, #57, #76, and #80) are identified with foreground stars, and the remaining three (#1, #4, and #77) are not identified with catalogued stars. #1 is identified with a faint photometric member candidate, source #4 with a faint background object and source #77 could be spurious (see Sect. 4).

5.2. Comparison with the PSPC observations

We have detected 73 sources already detected in Paper I and one reported in Dachs & Hummel (1996), while 88 sources from Paper I are missing from our list, although they fall in our field of view.

The large number of missing sources is not unexpected since the HRI is less sensitive than the PSPC. An estimate of the ability of HRI to detect the sources detected in the PSPC observation is shown in Fig. 6 where the PSPC count-rate vs. HRI offaxis angle is reported for all the JTX sources.[1] The sources not detected in the HRI are indicated with smaller symbols. As expected we detect the most intense sources, with a fuzzy threshold (offaxis dependent) that can be due to statistical fluctuations, different spectral shape or intrinsic variability.

The ROSAT PSPC observations were taken in 1993 (see Paper I). In order to explore X-ray flux variability on 3–4 year time scales we have compared X-ray fluxes measured by the HRI and the PSPC (in the $0.15-2.0$ keV band, as reported in Paper I). We have computed the ratios between the rates measured by the two instruments on each source, obtaining a median value of $\sim$ 0.4. This value is typical for thermal spectra with temperature in the $0.3-1.5$ keV interval and $N_H = 7\,10^{20}\mathrm{cm}^{-2}$ corresponding to the hydrogen column toward the cluster (see Paper I). The systematic uncertainty due to temperature range above is at most 15%. Since the HRI does not allow us to estimate spectral parameters, and to be consistent with Paper I, we have evaluated the $0.15-2.0$ keV flux observed with the HRI using the conversion factor in Paper I for PSPC data ($1.9\,10^{-11}\mathrm{erg\,cm}^{-2}$/count) and divided by 0.4. In this way we are making the same assumptions on source X-ray spectra done in Paper I and also assume that *on average* the intensity of the sources has not changed.

In Fig. 7 we show the scatter plot of HRI fluxes vs. those of Paper I. The solid line represents similar flux values, while the dashed lines represent variations of a factor two. In the figure we show all the sources detected by the two instruments, plus all the sources detected with the PSPC and undetected in the HRI observations. For these sources we have evaluated the upper limits to flux according to the wavelet detection algorithm at the positions of the PSPC sources. Most of the X-ray sources do not show variations larger than a factor two. The only sources that

[1] We note that the count rate of the source JTX115 reported in paper I, was wrong of a factor ten and the true PSPC count rate was 0.725 counts ks^{-2}, while X-ray flux and luminosity were correct

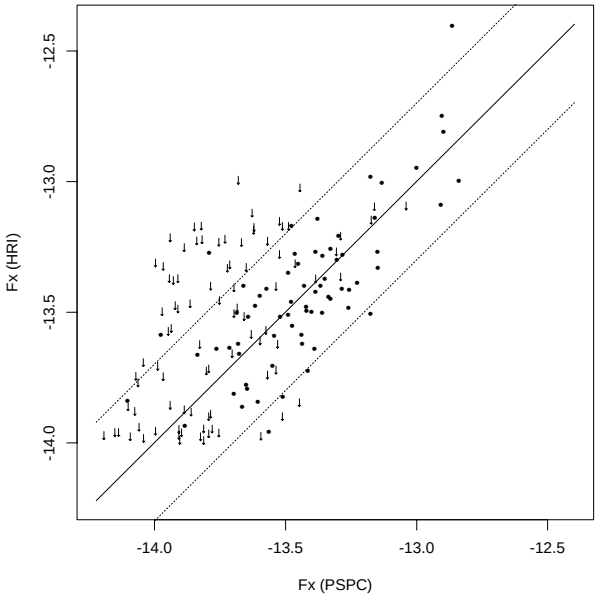

Fig. 7. HRI flux vs. PSPC flux (from Paper I). Solid line indicates the identity, while dashed lines represent variations of a factor two.

show large variations (apart from the B stars DK56 and DK15) are unidentified sources and have very faint counterparts. The HRI flux of the early B DK56 is about a factor three greater than the flux measured in the PSPC observation, it is possible that this variation is due to the UV contamination. Indeed if we compute the expected contamination of UV flux on the HRI-ROSAT detector, following the recipe of Barbera et al. (2000), based on laboratory measurements and observed stellar UV and X-ray spectra, for a B2 star of V=5.8 and E(B−V)=0.12 and hydrogen column of $7 \cdot 10^{20}$ cm^{-2} we obtain an expected count rate of the order of 5–6 $\cdot 10^{-3}$ cnt s^{-1} i.e. more than half of the observed counts. DK 15 presents a flux in the PSPC higher than in the HRI, so its variability seems real.

6. Discussion and conclusions

We have presented the results of an HRI observation on NGC 2516. We have detected 73 sources already detected with the PSPC (Paper I) and found 12 new X-ray sources. 47 of the detected sources are previously catalogued cluster members with colors in the $-0.2 <$ B-V < 1.0 range.

We present new photometric observations of the counterparts of sources unidentified with previously catalogued objects. 12 of these 28 sources have counterparts consistent with the low mass population of the cluster. The X-ray luminosity and the L_x/L_{bol} value for these stars is of the same order of that of the strongest emitters in the Pleiades, indicating that at least for these stars, metal abundance is not crucial in determining the peak X-ray activity level.

Notwithstanding the long exposure time we are not able to describe completely the X-ray properties of this cluster mainly for two reasons: the cluster is too far away so deeper exposures are needed to describe completely the X-ray luminosity functions and reliable membership is missing mainly at the low-end of the main sequence.

Given the limited sensitivity of our survey, our sample is severely biased towards strong emitters, therefore we cannot deduce the statistical properties of K and M stars in NGC 2516 and have merely established their peak levels of X-ray activity. We stress that we do not at present have an unbiased optical sample in these cooler stars, but on the contrary we identify stars as late-type cluster members thanks to their X-ray emission (together with the photometry). We expect that a number of JTX sources without catalogued counterparts are also K and M members of the cluster but with less extreme emission level. However we can state safely that there are K and M stars in NGC 2516 with the same activity level as K and M stars in more metal rich clusters of similar age, with $L_x/L_{bol} \sim 10^{-3}$. However we cannot yet say anything about the shape of the X-ray luminosity functions or if the saturation of X-ray activity occurs at a similar rotation rate in all these clusters.

Taking advantage of the time interval between the two different segments of the HRI exposures and of the PSPC exposure taken some years before, we have studied the X-ray variability properties of the stars of NGC 2516. To summarise, we find that only 3 out of the 47 (less than 10%) of the previously catalogued cluster members detected by the HRI (only one of the 27 stars redder than B−V=0.5) and only one of the 13 new faint photometric cluster candidates show variations greater than a factor two on six month time scales. None of these variable sources shows evidence for flares or other kinds of variability within each individual HRI segment. X-ray variability of cluster members on 3–4 year timescales also does not generally appear to exceed a factor of two. However, the more sensitive PSPC data in Paper I show that there is a range of X-ray flux at given colour among the late-type stars of NGC 2516 that exceeds an order of magnitude. We conclude that the most likely explanation for this is differences in rotation rate rather than magnetic activity cycles, unless those cycles have periods which considerably exceed the time base of our current X-ray observations.

Chandra and XMM observations, thanks to their effective area and high spatial resolution, together with detailed optical studies will allow us to explore lower X-ray luminosity and to better study the relevance of metallicity in determining the *distribution* of coronal properties.

Future, more sensitive, observations will help in exploring smaller amplitude variations and longer time scales.

Acknowledgements. GM and SS acknowledge financial support from ASI (Italian Space Agency), and MURST (Ministero della Università e della Ricerca Scientifica e Tecnologica) RDJ was a visiting astronomer at the Cerro Tololo Interamerican Observatory, operated by the Association of Universities for Research in Astronomy Inc., under contract to the National Science Foundation. MRT acknowledges a research studentship from the UK Particle Physics and Astronomy Research Council. We acknowledge the usage of the photographic data obtained using The UK Schmidt Telescope and the STScI digitization and compression. This research has made use of the Simbad database, operated at CDS, Strasbourg, France.

References

Barbera M., Collura A., Micela G, Murray S., Zombeck M., 2000, ApJ submitted

Branduardi-Raymont G., Mason K.O., Warwick R.S., et al., 1994, MNRAS 270, 947

Cameron L.M., 1985, A&A 147, 39

Dachs J., Hummel W., 1996, A&A 312, 818

Dachs J., Kabus H., 1989, A&AS 78, 25

Damiani F., Maggio A., Micela G., Sciortino S., 1997a, ApJ 483, 350

Damiani F., Maggio A., Micela G., Sciortino S., 1997b, ApJ 483, 370

Eggen O.J., 1972, ApJ 173, 63

Favata F., Micela G., Sciortino S., Vaiana G.S., 1992, A&A 256, 86

Favata F., Micela G., Sciortino S., 1995, A&A 298, 482

Guillout P., Sterzik M.F., Schmitt J.H.M.M., Motch C., Neuhaeuser R., 1998, A&A 337, 113

Hasinger G., Burg R., Giacconi R., et al., 1993, A&A 275, 1

Hawley S.L., Tourtellot J.G., Reid I.N., 1999, AJ 117, 1341

Jeffries R.D., Thurston M.R., Pye J.P., 1997, MNRAS 287, 350

Jeffries R.D., James D.J., Thurston M.R., 1998, MNRAS 300, 550

Landolt A., 1992, AJ 104, 340

Micela G., Maggio A., Vaiana G.S., 1992, ApJ 388, 171

Micela G., Sciortino S., Kashyap V., Harnden F.R. Jr., Rosner R., 1996, ApJS 102, 75

Micela G., Sciortino S., Harnden F.R. Jr., et al., 1999, A&A 341, 751

Pinsonneault M.H., Stauffer J.R., Soderblom D.R., Kiing J.R., Hanson R.B., 1998, ApJ 504, 192

Schmidt M., Hasinger G., Gunn J., et al., 1998, A&A 329, 495

Sciortino S., Damiani F., Favata F., Micela G., 1998, A&A 332, 825

Sciortino S., Favata F., Micela G., 1995, A&A 296, 370

Snowden S.L., 1998, ApJS 117, 233

Snowden S.L., McCammon D., Burrows D.N., Mendenhall J.A., 1994, ApJ 424, 714

Stark A.A., Gammie, C.F., Wilson, R.W., et al., 1992, ApJS 79, 77

Stauffer J.R., Caillault J.-P., Gagné M., Prosser C.F., Hartman L.W., 1994, ApJS 91, 625

Zombeck M.V., Conroy M., Harnden F.R. Jr., et al., 1990, Proceedings of the SPIE Conference on EUV, X-Ray and Gamma-Ray Instrumentation for Astronomy 1344, 267

Zombeck M.V., Barbera M., Collura A., Murray S.S., 1997, ApJ 487, L69